Oil Shale, 2024, Vol. 41, No. 3, pp. 145–162
doi: https://doi.org/10.3176/oil.2024.3.01
ISSN 0208-189X

Phase transformation and strength of hydrated circulating fluidised bed combustion ash sediment in an open environment over 15 years: implications for the long-term stability of ash waste plateaus

Alar Konist[(a)]*, Peeter Paaver[(b)], Tõnu Pihu[(a)], Kalle Kirsimäe[(b)]

[(a)] Department of Energy Technology, Tallinn University of Technology, Ehitajate tee 5, 19086 Tallinn, Estonia
[(b)] Department of Geology, Institute of Ecology and Earth Sciences, University of Tartu, Ravila 14A, 50411 Tartu, Estonia

Received 12 March 2024, accepted 12 July 2024, available online 5 August 2024

Abstract. *Low-temperature circulating fluidised bed combustion (CFBC) of oil shale results in Ca-rich ashes with low pozzolanic properties, raising concerns regarding the long-term stability of ash depositories. This paper presents findings from a long-term field study investigating the mineral and chemical transformations of total CFBC ash sediments over a 15-year period. The study reveals that the pozzolanic properties of CFBC ashes are primarily influenced by the formation of Ca-Al sulphate mineral ettringite and the compactness of sediment. The compaction of ashes during deposition contributes to the development of a dense microstructure, providing uniaxial compressive strength that exceeds 20 MPa. Our findings suggest that compacted and hydrated CFBC ashes are sufficiently stable in ash deposits, holding promise as a sustainable alternative for cement-free construction materials.*

Keywords**:** *CFBC ashes, strength development, long-term stability.*

1. Introduction

Estonian oil shale, which is one of the best-quality oil shales with a calorific value of 7–9 MJ/kg, has been and still is the largest industrially exploited oil shale resource in the world. The oil shale industry accounts for more than 70% of the Estonian energy sector, with approximately 41% of planned oil shale being consumed by direct combustion in thermal power plants [1]. Pulverised combustion (PC) and circulating fluidised bed combustion (CFBC)

* Corresponding author, alar.konist@taltech.ee

technologies are used for power production. The oil shale received at power plants is characterised by moisture levels between 9 to 13%, ash content ranging from 45 to 57%, mineral carbon dioxide content of 16 to 21%, sulphur levels between 1.5 to 2.1%, and a lower heating value of 7.3 to 8.7 MJ/kg [2]. The heating value of oil shale used for PC units that were closed in 2018 was 7.6 MJ/kg [3].

Oil shale processing generates a large volume of solid alkaline waste ash, even at reduced mining rates. In 2022, ca 6 Mt of oil shale processing waste was produced per 10.7 Mt of oil shale. The utilisation of solid wastes from oil shale processing is challenging, requiring additional investments, and ash valorisation remains one of the most contentious issues in Estonia's energy sector. Secondary beneficial reuse of oil shale ashes is minimal, accounting for less than 2% of the total ash output. Consequently, millions of tonnes of ashes are annually dumped in large, up to 45 m high waste depositories, covering more than 20 km^2 next to the two major power plants [4–6].

The buildup of steeply sloped, dozens of metres high plateaus has been facilitated by the cementitious properties of oil shale ash residues, allowing also the use of fine fractions of ash feed, particularly those from PC boilers, as raw materials for Portland cement and gas-concrete block production [7]. Additionally, oil shale ashes have been employed as a stabilizing agent in road constructions and as a liming agent for acidic soils due to their high free CaO content [8]. However, since 2004, high-temperature (>1200–1400 °C) PC boilers have been gradually replaced with more effective and less CO_2-intensive CFBC boilers firing oil shale at temperatures of 800–850 °C [9]. CFBC technology is more efficient [10, 11] compared to PC boilers. Furthermore, CFBC technology favours almost complete SO_2 capture through the formation of the solid $CaSO_4$ (anhydrite) phase in a reaction between free CaO and SO_2 or direct sulphation [1]. Similar ashes are also produced in novel shale oil retorts using solid heat carrier (SHC) technology, such as in the Enefit-280 retort, where spent shale acts as a heat carrier and flue gases are additionally combusted below 800 °C [12, 13].

The transition to lower-temperature firing technology and the consequent increase in $CaSO_4$ content have negatively affected the physical and chemical characteristics of oil shale ashes [14–16]. In addition to the higher content of undecomposed carbonate and Ca-sulphate, the formation of secondary Ca-rich phases has moved away from Ca-silicates, resulting in significantly lower cementitious-pozzolanic properties of CFBC ashes compared to earlier high-temperature PC ashes [17]. This change has narrowed down the reusability of ashes and has caused problems with ash deposition on ash plateaus since the large-scale employment of CFBC technology [14].

Another problem arising from the hydraulic deposition of CFBC ashes used in Estonian power plants is the strong grain-size separation along the flow path [14]. The grain-size distribution of CFBC ashes varies in a much wider range compared to rather uniform PC ashes [18]. While in PC ashes the content

of CaO reaches its maximum (ca 25–30%) in furnace ashes and decreases along the ash collection path all the way to the electrostatic precipitators, then in CFBC ashes, the content of lime in the bottom ash is lower (ca 10–15%) and reaches its maximum in the economiser/air-preheater zone before decreasing through the fields of electrostatic precipitators [19]. As a result, the particles deposited at the entrance of the ash deposition channels on plateaus are composed of coarse-grained irregular size aggregates of undecomposed calcite grains and larger Ca-sulphate particles, which mostly originate from the CFBC bottom ash. The coarse structure and smaller proportion of free lime in this sediment fail to provide the necessary cementation, causing concerns about the long-term stability of ash plateaus [4, 14, 20].

In this contribution, we report the results of a long-term field experiment to study the mineral and chemical transformations as well as the geotechnical properties of CFBC ash sediment under an open environment over 15 years. We aimed at testing the long-term performance of hydrated CFBC ash sediment and its potential influence on the integrity of ash plateaus.

2. Materials and methods

The CFBC hydration experiment was set up on 4 November 2008. A test block with the dimensions of 1200 × 590 × 230 mm was made by mixing CFBC total ash from the Balti Power Plant (energy unit No. 11) with water at the ratio of 0.48 L/kg. The chosen water ratio corresponded to the water demand of CFBC ash paste, allowing for complete hydration of the ash mixture. The mixture was then compacted with a plate vibrator (Fig. 1). The box with the test block was left outdoors in Kopli, Tallinn. Thermocouples were installed in the test block to monitor the mixture temperature during the initial hydration of the ash mixture over five months, in parallel with the outside air temperature.

Samples from the outer and inner parts of the test block were collected in February 2009, March 2009, September 2009, April 2017 and November 2024. These samples were studied for the mineral and chemical composition as well as microstructure development, using X-ray diffraction (XRD) and analytical scanning electron microscopy (SEM). XRD analysis of ash deposit sediment samples was carried out on powdered unoriented preparations with a Bruker D8 Advance diffractometer using primary monochromator filtered Cu–Kα radiation and the LynxEye detector system. Rietveld analysis of XRD patterns was performed using the Topas code, ensuring a relative error of quantification better than 10% for major phases (content >5 wt%) and better than 20% for minor phases (content <5 wt%). The grain-size distribution of raw ash was measured by sedimentation analysis and the chemical composition was determined using standard gravimetric analysis. Pressed pellets were used to determine the chemical composition of hydrated ash by X-ray fluorescence spectroscopy (XRF) using a Rigaku Primus II spectrometer. The loss on

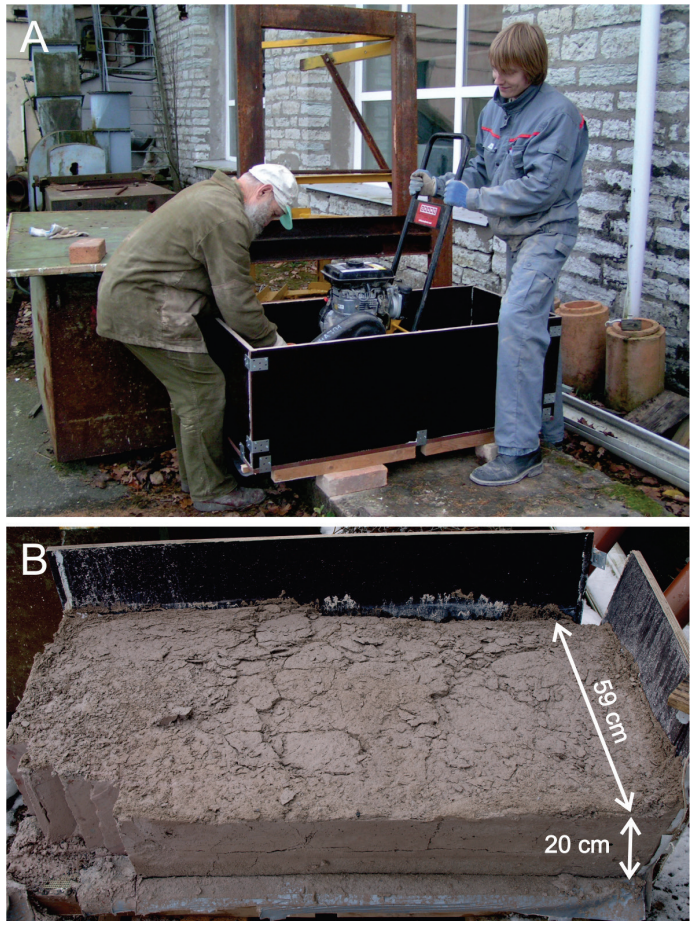

Fig. 1. Setup of the CFBC ash hydration experiment on 4 November 2008 (A). View of the test block during the sampling on 18 March 2009 (B). Samples were cut with a grinder from a corner of the block.

ignition (LOI) of the samples was determined by heating at 950 °C for 2 h.

SEM imaging and chemical analyses of the broken surfaces of samples were carried out with a Zeiss EVO 15MA scanning electron microscope equipped with an Oxford X-MAX energy dispersive detector system (EDS) and AZTEC software for element analysis and distribution mapping.

During the final sampling in November 2024, cylindrical monolith samples with a diameter of 64 mm (Fig. 2) were drilled with a diamond drill and tested for uniaxial compressive strength measurements under continuous loading (20 kPa/s) until the specimen broke, utilising a Matest Servo-Plus Evolution press.

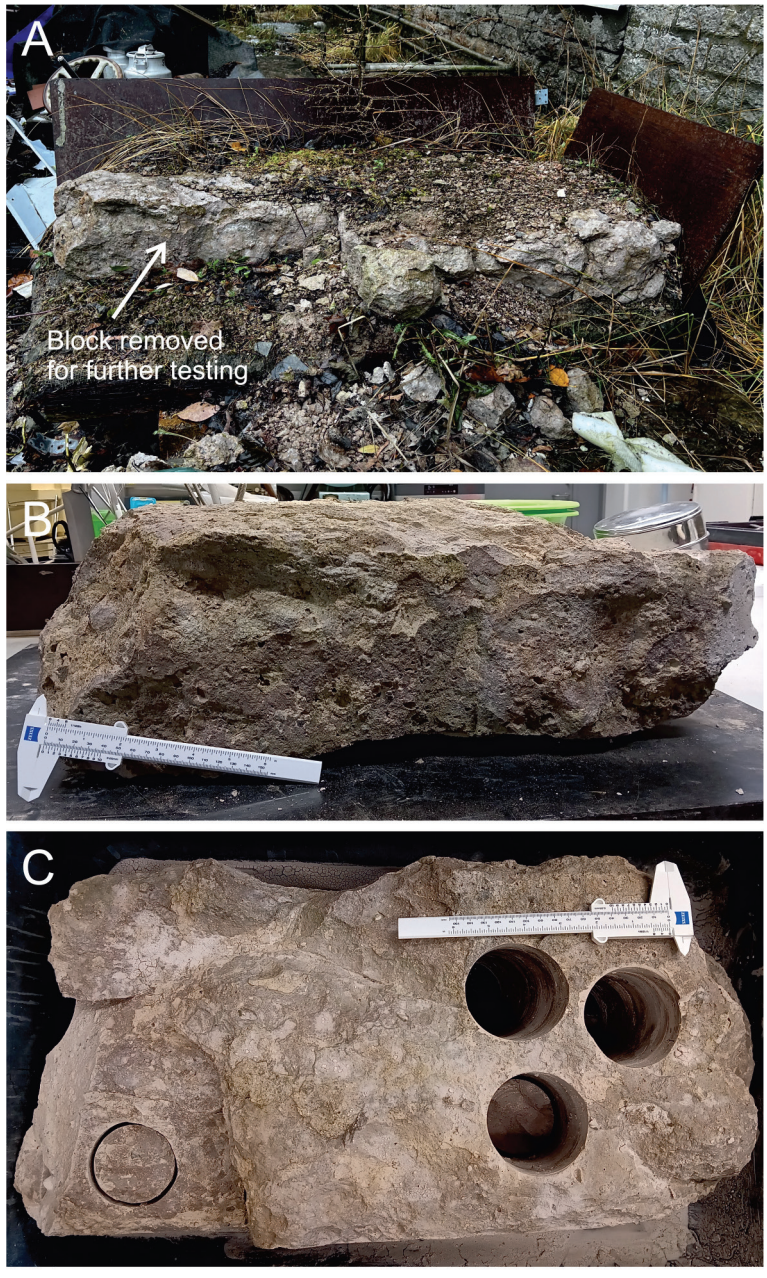

Fig. 2. Test block during the final sampling on 24 November 2023 (A). Block extracted from the field. Side view (B) and top view with drill-holes made for monoliths used for uniaxial compressive strength testing (C).

3. Results

The inside temperature of the test block peaked at 54 °C during the initial lime slaking but dropped quickly close to the outside air temperature. After a week, the outside and inside temperature trends of the block were nearly parallel. During the relatively mild winter of 2008–2009, the minimum registered inside temperature was –5.5 °C. Over the monitoring period, it went through several freezing-thawing cycles (Fig. 3).

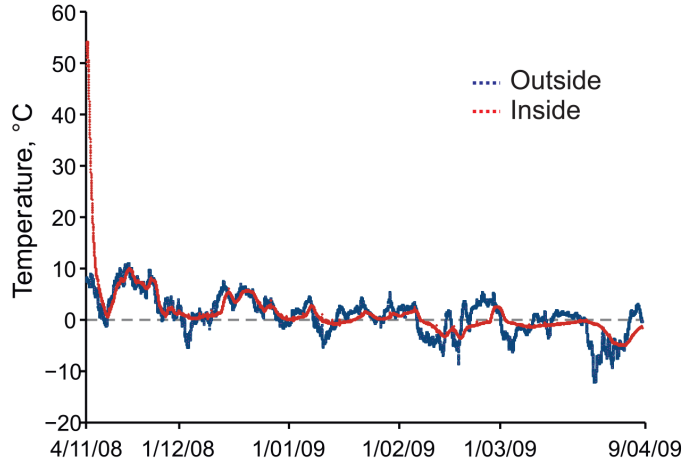

Fig. 3. Outside and inside temperature trends of the test block monitored over a five-month period at the beginning of the experiment.

The grain size of raw ash (Fig. 4) shows that total ash is a poorly sorted material with a median grain size of about 0.1 to 0.3 mm.

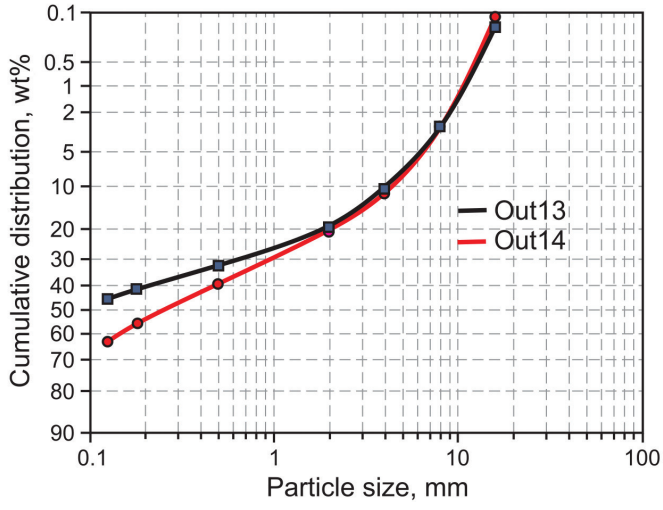

Fig. 4. Cumulative grain-size distribution of two raw CFBC samples (Out13 and Out14) used for making the test block mixture.

The mineral composition of fresh unhydrated CFBC ashes was dominated by lime (9.2 wt%), anhydrite (12.49 wt%), calcite (19.9 wt%), quartz (13.4 wt%), K-feldspar (9.8 wt%), K-mica (4.6 wt%), periclase (3.9 wt%), as well as about 11.9 wt% of secondary Ca-Mg silicates formed upon firing (C_2S, merwinite, akermanite and wollastonite). Hydrated ashes consisted of calcite-portlandite, terrigenous-residual phases (quartz, K-feldspar, K-mica), secondary Ca-Mg silicates, and secondary hydrate phases – ettringite and hydrotalcite, with minor hematite, periclase and its hydration product brucite (Table 1, Figs 5–7). The calcite content in hydrated ashes varied from 30 to 37 wt%, and its apparent content increased slightly over time (Fig. 5), while the portlandite content decreased. The content of terrigenous phases was stable between 25.5 and 20.5 wt%, and the Ca-Mg-silicates accounted for 5 to 7 wt% of the crystalline phases. Ettringite content was, on average, between 15 and 20.5 wt%, with a somewhat higher share observed in samples taken from the inner parts of the test block (Figs 6, 7). The hydrotalcite content ranged from 4 to 8 wt%, showing a subtle increase over the hydration time (Table 1).

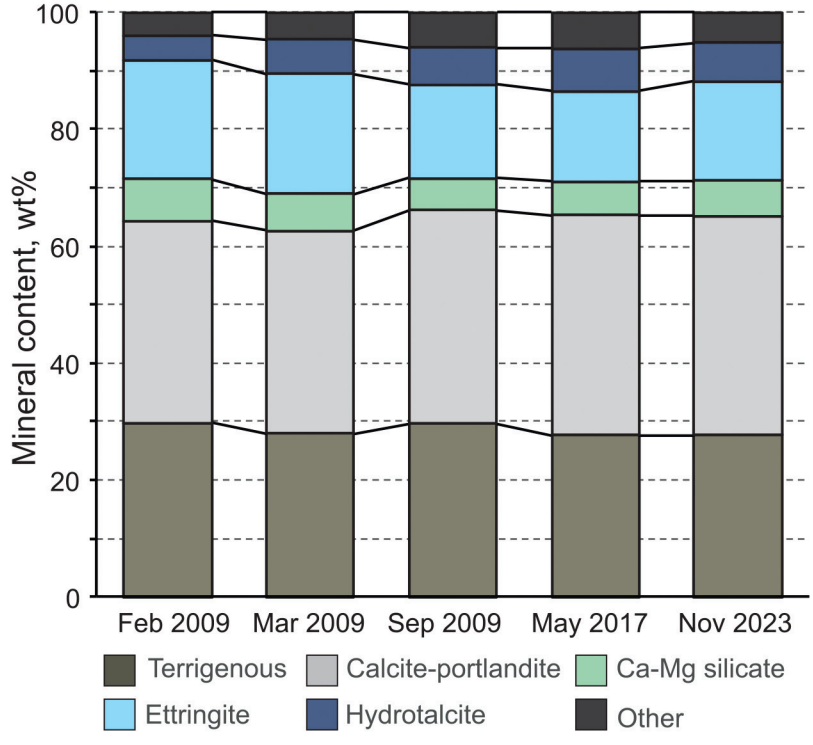

Fig. 5. Average mineral composition of hydrated ash.

Table 1. Mineral composition of the studied samples, wt%, tr <0.5 wt%. Sample BEJ-3 collected from the surface layer of the test block in February 2009. Samples T2-1, T2-2, T2-3 and T2-4 collected in March 2009, representing a cross-section of the block from a lower corner of the block shown in Fig. 1B. Samples STI07 and STI08 retrieved in September 2009 from the same place as the previous set. Samples KAS17-1 and KAS17-2 drilled from the test block in April 2017. Samples KAS23 10–15, 5–10, 2–5 and 0–2 sampled from drilled monoliths in November 2024, representing a depth profile through the test block from bottom to top. Numbers 10–15, 5–10, 2–5 and 2–0 indicate depth in cm

Sample	Sample date	Quartz	K-feldspar	K-mica	Calcite	Dolomite	Apatite	Portlandite	Periclase	Brucite	Nordstrandite	C_2S	Akermanite	Merwinite	Wollastonite	Ettringite	Hydrotalcite	Hematite	Gypsum
BEJ-3	12.02.2009	13.4	9.9	4.6	30.2	0.8	0.9	4.2	1.4	0.4	tr	2.0	2.0	0.5	2.6	20.2	4.3	2.1	tr
T2-1	18.03.2009	13.6	9.7	4.6	33.2	0.8	0.9	1.8	1.3	0.8	0.5	1.3	2.0	tr	2.5	19.6	4.6	2.0	tr
T2-2	18.03.2009	13.7	9.3	4.5	32.8	0.8	0.8	1.8	1.3	0.9	0.5	1.2	1.9	tr	2.5	20.6	4.9	2.0	tr
T2-3	18.03.2009	12.1	7.7	3.2	31.5	1.4	1.1	2.8	tr	1.5	0.7	1.6	1.3	0.5	2.2	24.6	6.0	1.5	tr
T2-4	18.03.2009	12.6	9.3	3.2	31.2	1.0	1.3	3.1	0.8	1.5	1.3	1.2	2.5	0.9	3.0	17.0	8.2	1.8	tr
STI07	29.09.2009	13.9	9.6	3.3	35.2	0.9	1.4	1.6	0.7	1.6	2.1	1.1	1.3	0.5	2.5	15.5	6.7	1.8	tr
STI08	29.09.2009	13.0	8.7	6.1	34.7	0.9	1.2	1.3	0.5	2.1	1.4	1.6	1.4	tr	2.2	16.3	6.1	1.8	tr
KAS17-1	15.05.2017	12.8	8.8	3.2	36.6	0.6	1.4	1.6	0.6	1.7	2.2	1.1	1.3	0.5	2.5	15.7	6.8	1.8	tr
KAS17-2	15.05.2017	13.2	9.3	3.2	34.7	0.8	1.6	1.8	0.5	1.5	1.9	1.0	1.7	0.8	2.6	14.8	7.8	2.1	tr
KAS23 10–15	24.11.2023	13.2	8.8	3.2	36.9	0.6	1.4	1.2	0.6	1.7	2.2	1.1	1.3	0.5	2.5	15.5	6.8	1.7	tr
KAS23 5–10	24.11.2023	11.7	8.1	3.3	33.4	1.5	1.1	2.7	tr	1.5	0.8	1.6	1.3	0.5	2.2	22.7	6.1	1.4	n.a
KAS23 2–5	24.11.2023	12.1	9.6	3.4	33.8	1.1	1.3	3.2	0.7	1.6	1.2	1.2	2.4	0.9	2.9	15.9	6.9	1.8	n.a
KAS23 0–2	24.11.2023	13.4	8.8	5.3	37.6	0.9	1.2	0.7	0.5	2.0	1.4	1.6	1.4	tr	2.5	13.5	6.2	1.9	tr

tr – traces, n.a – not available

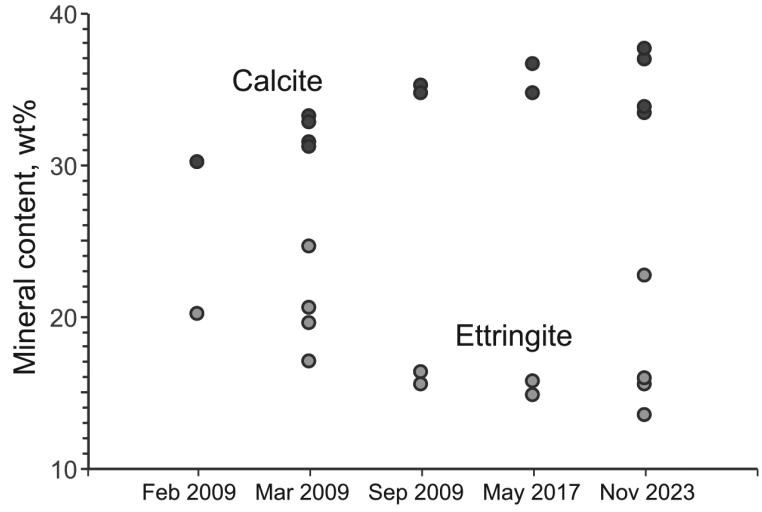

Fig. 6. Changes in calcite and ettringite contents over the experiment period.

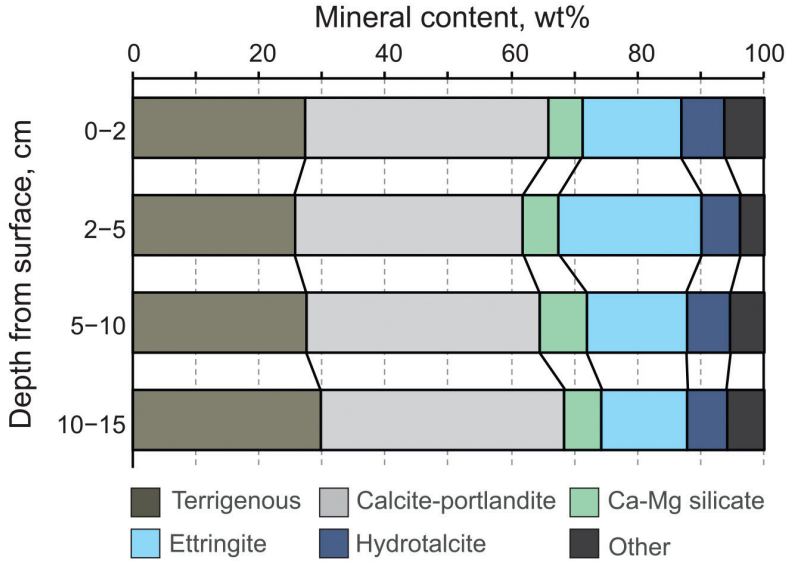

Fig. 7. Variation in mineral composition through the block extracted during the sampling on 24 November 2023.

Variation in the mineral composition in a profile sampled in November 2023 through the whole thickness of the test block showed higher calcite content, 36.9 and 37.7 wt% at the upper and lower contacts of the block, respectively. In contrast, the ettringite content was lowest, 15.5 and 13.5 wt%, respectively, but reached nearly 23 wt% in the middle section (Fig. 7).

Table 2. Chemical composition of average raw ash and hydrated samples, wt% (see sampling dates and sample explanations in Table 1)

Sample	SiO_2	Al_2O_3	TiO_2	Fe_2O_3	MnO	CaO	MgO	Na_2O	K_2O	P_2O_5	SO_3	LOI
Average raw ash	24.88	9.48	n.a	2.12	n.a	37.18	5.04	0.06	2.54	n.a	n.a	11.65
KAS23 0–2	27.73	6.98	0.27	3.11	0.06	24.62	4.62	0.03	2.11	0.50	2.77	26.82
KAS23 2–5	27.42	6.64	0.27	2.14	0.05	24.96	5.03	0.05	2.03	0.55	3.04	28.39
KAS23 5–10	26.98	6.60	0.29	1.52	0.06	23.60	4.13	0.06	1.76	0.46	4.34	31.13
KAS23 10–15	26.93	6.87	0.27	3.03	0.07	24.34	4.75	0.04	1.87	0.59	3.15	27.74

n.a – not available

The chemical composition of hydrated ash samples was measured in the samples taken during the last sampling in November 2023. The chemical composition of both the raw and hydrated ashes is shown in Table 2. The CaO content varied from 23.6 to 37.18 wt%, while the content of SiO_2 was between 24.9–27.7 wt%. The contents of Al_2O_3, MgO and Fe_2O_3 were in the range of 6.6–9.5, 4.1–5.0 and 1.5–3.1 wt%, respectively. The SO_3 content varied between 2.8–3.2 wt%, and LOI ranged from 11.7 to 30.0 wt%.

The uniaxial compressive strength of the CFBC ash pastes after 15 years of staying outdoors yielded in three tested specimens at 24.0, 21.8 and 18.5 MPa, representing the upper, middle and lower parts of the test block, respectively.

Microstructure analysis of ash sediments sampled at different times throughout the 15-year period is shown in SEM images (Figs 8, 9). The material sampled at the beginning of the experiment in February 2009 was composed of tightly packed granular material over- and intergrown by short ettringite crystals and authigenic calcite aggregates (Fig. 8A, B). By September 2009, the material had developed into compact, fine-grained masses, filling the space between unreacted/resistant ash particles and their fragments (Fig. 8C).

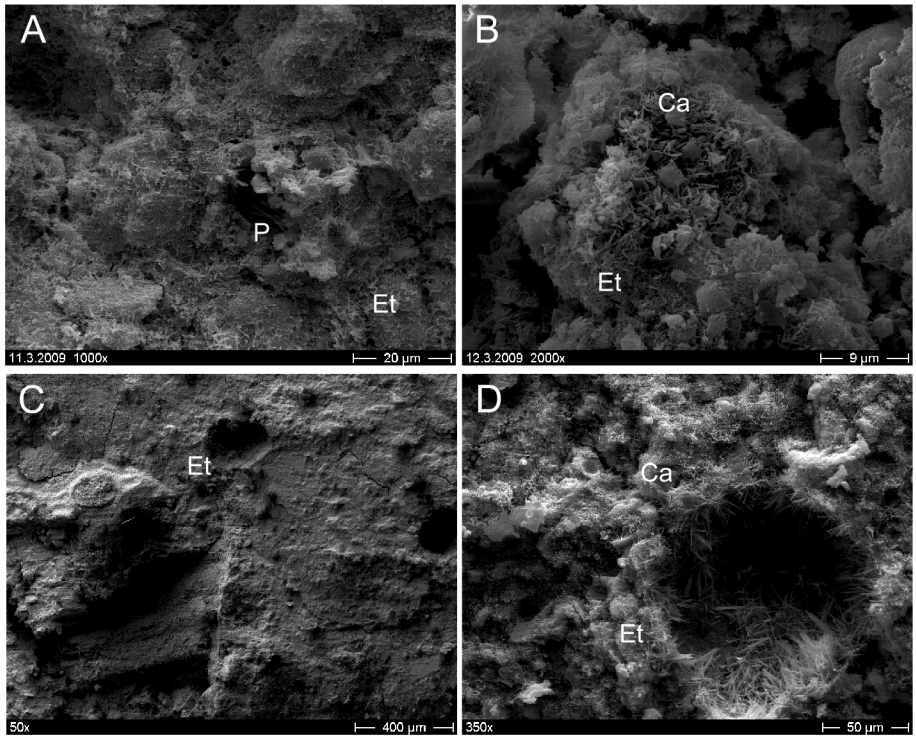

Fig. 8. Scanning electron images of the hydrated ash microstructure at the beginning of the experiment in February 2009 (A, B). Note that tightly packed granular material is overgrown with short ettringite (Et) crystals and authigenic calcite (Ca) aggregates. The compact fine-grained mass is filled with abundant void-filling ettringite crystal aggregates and portlandite (P) (C, D).

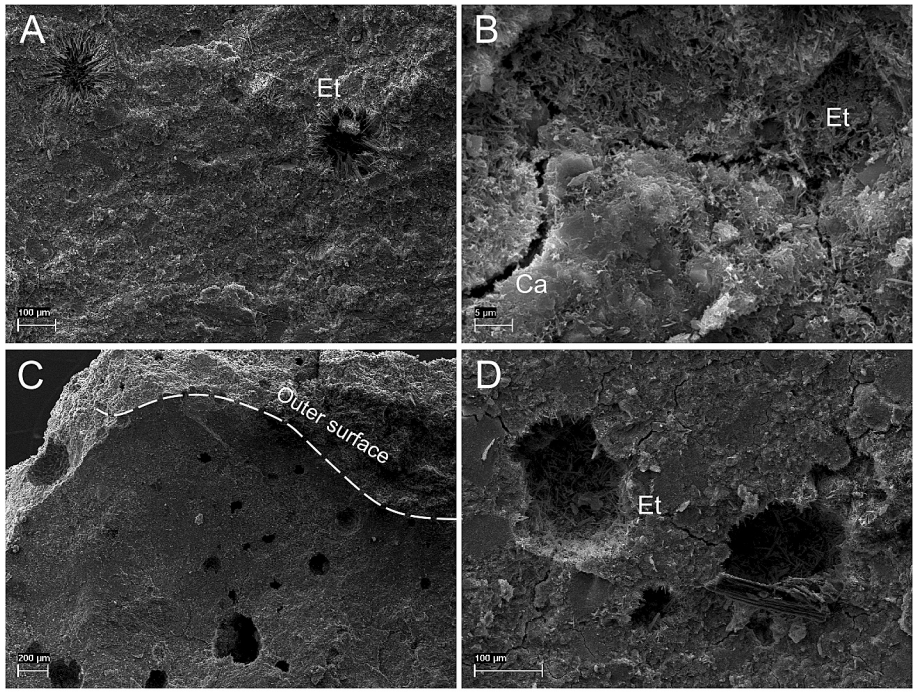

Fig. 9. Microstructure of the samples taken in November 2023 shows a compact matrix with abundant ettringite (Et) filled pores/voids (A, B) from ca 10 cm depth from the block surface. Note that voids are empty in the uppermost leached layer, indicating ettringite dissolution (C), but ettringite is present in the same specimen at ca 1 cm depth from the surface (D).

Occasional pores/voids were filled with radially inward-growing elongated lath-shaped ettringite crystal aggregates (Fig. 8D). The microstructure of the samples collected in November 2023 showed differences between samples taken from the upper surface of the test block and those from the middle of the test block. The latter had retained a similar compacted matrix with abundant ettringite-filled pores/voids (Fig. 9A, B). Samples from the surface, however, exhibited leaching, and the ettringite aggregate fillings had disappeared from the voids. Nevertheless, the leached zone was only a few cm thick, and voids, with partly preserved ettringite aggregates, appeared already at a 0.5-cm depth below the test block surface (Fig. 9B, C).

4. Discussion

It has been commonly considered that the pozzolanic properties of oil shale ashes depend mainly on the composition and content of secondary Ca-silicate phases (belite – C_2S), free lime (CaO), and the pozzolanic properties of the silicate glass phase [15, 21]. Already Arro et al. [22] noticed that though the

hydrated CFBC electrostatic precipitator ash still had the highest binding capacity and compressive strength, the final compressive strength of hydrated PC ash mortars (15.4 MPa) was three times higher than that of the same fractions of CFBC ashes. This disparity is directly related to the content of potential binding phases and their distribution between different grain-size fractions. The high-temperature PC ensured the complete thermal dissociation of the carbonate phases as well as vigorous reactions between free CaO and silicate phases, resulting in the formation of multiple potential binding phases: free CaO, belite (β-C_2S) and amorphous glass. These accounted for about 70–80% of the phase composition in the fine fractions of PC ashes collected at electrostatic precipitator filters, but the content of these phases was already as high as 50–60% in the coarse-grained bottom ash fractions of PC ashes [19]. This is at least two times higher than the content of reactive phases in CFCB ashes, forming at the temperatures of 800–850 °C [19, 23, 24]. In addition to the significantly lower free CaO content in CFBC ashes (15–20 wt% compared to 30 wt% in PC ashes), the amount of secondary Ca-silicate phases and amorphous glass phases is at least twice as low in low-temperature CFBC ashes, pointing at their lower pozzolanic potential.

During the hydration of oil shale CFBC ashes and strength development, the slaking of lime, which leads to the formation of Ca-hydroxide (portlandite), is the fastest reaction, occurring over the first 24–48 hours. However, its subsequent carbonation by CO_2 uptake can go on for decades, depending on the availability of CO_2 [4, 5, 25]. In the next stage, the dissolution of the Ca-sulphate phase (anhydrite) and the establishment of alkaline pore solution initiate the precipitation of ettringite ($Ca_6Al_2(SO_4)_3(OH)_{12}\cdot 26H_2O$), followed by the formation of hydrocalumite and/or hydrotalcite type phase and gypsum [25, 26]. In addition, Leben et al. [4] have shown that in ash depository materials composed mainly of PC ashes, the hydration of secondary Ca-silicate minerals, such as C_2S and Si-Ca-Al glassy phases, can form a C-S-H type semi-amorphous phase that provides additional binding capacity to the oil shale ash sediment, at least in the long term. However, in CFBC ashes, the binding properties seem to be controlled mainly by free CaO and its hydration/carbonation, as well as the precipitation of secondary Ca(Al)-sulphate-hydrate phases, particularly ettringite. As a result, CFBC ashes do not appear to produce as good pozzolanic properties as high-temperature PC ashes.

The phase composition of the test block with high ettringite content varying between 15–20 wt% is remarkably similar to the sediments in the upper part of the Balti Power Plant ash deposit, mainly composed of ash residues from CFBC boilers [4]. In this sense, the test block sediment would have behaved similarly to typical hydrated CFBC ashes, where uniaxial strength remains <10 MPa [22]. However, the 20–22 MPa uniaxial strength values of the CFBC paste in our experiment indicate the remarkable performance of the hydrated CFBC ashes even after staying in an open environment for 15 years. On the one hand, this could be attributed to a more extended hydration

period than usually tested (i.e. compressive strength is typically assessed after 7 and 28 days of hydration). Nevertheless, Paaver et al. [24] monitored the strength performance of CFBC pastes over a three-month period, with the pastes reaching only 7–9 MPa compressive strength after 90 days of curing, whereas the strength increase slowed down between 28 and 90 days of curing. On the other hand, Paaver et al. [24, 27] showed that even a short period of mechanical activation of the Ca-rich oil shale CFBC ashes yielded a nearly tenfold improvement in the compressive strength of hydrated fly ash pastes, topping at 60 MPa after 90 days without any chemical activation or blending, and that mechanically activated CFBC ashes performed as an active binder, allowing a high volume of ordinary Portland cement replacement.

Paaver et al. [24] suggested that mechanical activation facilitated the fragmentation of large irregular flaky porous lumps and aggregates characteristic of CFBC ashes, improving reactivity by creating a finer grain size, larger surface area, and disintegration of compact $CaSO_4$ shells on unreacted CaO cores. As a result, the enhancement of mechanical strength was achieved by a significantly more compact microstructure, where the pore space between unreacted particles is completely filled with dense webs of ettringite crystallites, calcite from portlandite carbonation, and possibly a gel-like Ca-Al-Si phase. This also suggests that in compacted CFBC ashes, the cementitious properties are mainly controlled by the formation of crystalline ettringite, and the phase development in activated CFBC ashes is similar to that in calcium sulphoaluminate (CSA) cements, where the hydration of ye'elimite in the presence of gypsum produces ettringite and nanocrystalline Al-hydroxide [28–32]. In CFBC ashes, ettringite forms at the expense of reactive Ca, anhydrite and Al-bearing phases (glass, clay minerals, feldspars), possibly limited by the availability of reactive Al phases [25].

In this sense, our experimental results showing high compressive strengths of the hydrated CFBC ash material, exceeding those achieved in other experiments [7, 16], can be explained by using the total ash composed of varying grain-size fractions and compacting the ash paste with a vibrating plate during the experimental test block preparation (Fig. 1). This provided a compact structure where the rapidly growing ettringite formed a dense mesh of interlocking crystallites, providing mechanical strength to the hydrated ash block. However, it should be considered that ettringite is a metastable phase that dissolves incongruently to gypsum, (amorphous) Al-hydroxide and Ca-carbonate when pH drops below 10.7 [33]. Nevertheless, in the hydrated ash sediments, portlandite dissolution equilibrium controls the solution pH at ca 12, which is well above the ettringite stability limit, ensuring the stability of ettringite. The preservation of portlandite in the test block over 15 years indicates that the diffusion of atmospheric CO_2 has been, similar to large ash plateau deposits [4, 34, 35], extremely limited in the compacted ash sediments. Consequently, the carbonation of portlandite, and the leaching and destruction of ettringite have affected only a limited surface layer of the sample.

5. Conclusions

Results of this study show that, similar to PC ash deposits, unfractionated total CFBC ash yields significant compressive strength upon hydration, reaching 20 MPa, and the ash sediments are capable of retaining their geotechnical integrity over extended periods of time, though the mode of mineralization providing the mechanical strength in CFBC ashes is different. To achieve a compact structure and higher strength values, it is important to avoid grain-size separation of the ash pulp in the hydraulic deposition system. Additionally, the results of this study highlight that compacted and hydrated total CFBC ash, potentially in combination with accelerated carbonation [36] is a promising material for making cement-free construction materials.

Acknowledgements

This study was supported by the project ÕÜF-14 'Increasing the knowledge intensity of Ida-Viru entrepreneurship', co-funded by the European Union, and by the Ministry of Education and Research through the Centre of Excellence in Circular Economy for Strategic Mineral and Carbon Resources (01.01.2024–31.12.2030, TK228). The publication costs of this article were partially covered by the Estonian Academy of Sciences.

References

1. Baqain, M., Rüstü Yörük, C., Nešumajev, D., Järvik, O., Konist, A. Ash characterisation formed under different oxy-fuel circulating fluidized bed conditions. *Fuel*, 2023, **338**, 127244. https://doi.org/10.1016/j.fuel.2022.127244
2. Konist, A. Investigation of fouling and corrosion of low-temperature reheater in a CFBC boiler. *Fuel*, 2023, **338**, 127373. https://doi.org/10.1016/j.fuel.2022.127373
3. Konist, A., Maaten, B., Loo, L., Neshumayev, D., Pihu, T. Mineral sequestration of CO_2 by carbonation of Ca-rich oil shale ash in natural conditions. *Oil Shale*, 2016, **33**(3), 248–259. https://doi.org/10.3176/oil.2016.3.04
4. Leben, K., Mõtlep, R., Paaver, P., Konist, A., Pihu, T., Paiste, P., Heinmaa, I., Nurk, G., Anthony, E. J., Kirsimäe, K. Long-term mineral transformation of Ca-rich oil shale ash waste. *Sci. Total Environ.*, 2019, **658**, 1404–1415. https://doi.org/10.1016/j.scitotenv.2018.12.326
5. Mõtlep, R., Sild, T., Puura, E., Kirsimäe, K. Composition, diagenetic transformation and alkalinity potential of oil shale ash sediments. *J. Hazard. Mater.*, 2010, **184**(1–3), 567–573. https://doi.org/10.1016/j.jhazmat.2010.08.073
6. Pihu, T., Konist, A., Puura, E., Liira, M., Kirsimäe, K. Properties and environmental impact of oil shale ash landfills. *Oil Shale*, 2019, **36**(2), 257–270. https://doi.org/10.3176/oil.2019.2.01

7. Raado, L.-M., Hain, T., Liisma, E., Kuusik, R. Composition and properties of oil shale ash concrete. *Oil Shale*, 2014, **31**(2), 147–160. https://doi.org/10.3176/oil.2014.2.05
8. Kuusik, R., Uibu, M., Trikkel, A., Kaljuvee, T. Reuse of waste ashes formed at oil shale based power industry in Estonia. In: *Waste Management and the Environment III* (Popov, V., Kungolos, A. G., Brebbia, C. A., Itoh, H., eds). WIT Press, Southampton, 2006, 111–120. https://doi.org/10.2495/WM060131
9. Ots, A. *Oil Shale Fuel Combustion*. Tallinna Raamatutrükikoda, Tallinn, 2006.
10. Konist, A., Järvik, O., Pikkor, H., Neshumayev, D., Pihu, T. Utilization of pyrolytic wastewater in oil shale fired CFBC boiler. *J. Clean. Prod.*, 2019, **234**, 487–493. https://doi.org/10.1016/j.jclepro.2019.06.213
11. Aurela, M., Mylläri, F., Konist, A., Saarikoski, S., Olin, M., Simonen, P., Bloss, M., Neshumayev, D., Salo, L., Maasikmets, M., Sipilä, M., Dal Maso, M., Keskinen, J., Timonen, H., Rönkkö, T. Chemical and physical characterization of oil shale combustion emissions in Estonia. *Atmos. Environ.: X*, 2021, **12**, 100139. https://doi.org/10.1016/j.aeaoa.2021.100139
12. Paaver, P., Paiste, P., Mõtlep, R., Kirsimäe, K. Self-cementing properties and alkali activation of Enefit280 solid heat carrier retorting ash. *Oil Shale*, 2017, **34**(3), 263–278. https://doi.org/10.3176/oil.2017.3.05
13. Neshumayev, D., Pihu, T., Siirde, A., Järvik, O., Konist, A. Solid heat carrier oil shale retorting technology with integrated CFB technology. *Oil Shale*, 2019, **36**(2S), 99–113. https://doi.org/10.3176/oil.2019.2S.02
14. Pihu, T., Arro, H., Prikk, A., Rootamm, R., Konist, A., Kirsimäe, K., Liira, M., Mõtlep, R. Oil shale CFBC ash cementation properties in ash fields. *Fuel*, 2012, **93**, 172–180. https://doi.org/10.1016/j.fuel.2011.08.050
15. Raado, L.-M., Kuusik, R., Hain, T., Uibu, M., Somelar, P. Oil shale ash based stone formation – hydration, hardening dynamics and phase transformations. *Oil Shale*, 2014, **31**(1), 91–101. https://doi.org/10.3176/oil.2014.1.09
16. Usta, M. C., Yörük, C. R., Hain, T., Paaver, P., Snellings, R., Rozov, E., Gregor, A., Kuusik, R., Trikkel, A., Uibu, M. Evaluation of new applications of oil shale ashes in building materials. *Minerals*, 2020, **10**(9), 765. https://doi.org/10.3390/Min10090765
17. Paaver, P., Paiste, P., Liira, M., Kirsimäe, K. Alkali activation of Estonian Ca-rich oil shale ashes: a synthesis. *Oil Shale*, 2019, **36**(2S), 214–225. https://doi.org/10.3176/oil.2019.2S.11
18. Kuusik, R., Uibu, M., Kirsimäe, K. Characterization of oil shale ashes formed at industrial-scale CFBC boilers. *Oil Shale*, 2005, **22**(4S), 407–419. https://doi.org/10.3176/oil.2005.4S.04
19. Bityukova, L., Mõtlep, R., Kirsimäe, K. Composition of oil shale ashes from pulverized firing and circulating fluidized-bed boiler in Narva thermal power plants, Estonia. *Oil Shale*, 2010, **27**(4), 339–353. https://doi.org/10.3176/oil.2010.4.07
20. Konist, A., Valtsev, A., Loo, L., Pihu, T., Liira, M., Kirsimäe, K. Influence of oxy-fuel combustion of Ca-rich oil shale fuel on carbonate stability

and ash composition. *Fuel*, 2015, **139**, 671–677. https://doi.org/10.1016/j.fuel.2014.09.050

21. Uibu, M., Somelar, P., Raado, L.-M., Irha, N., Hain, T., Koroljova, A., Kuusik, R. Oil shale ash based backfilling concrete – strength development, mineral transformations and leachability. *Constr. Build. Mater.*, 2016, **102**(1), 620–630. https://doi.org/10.1016/j.conbuildmat.2015.10.197
22. Arro, H., Pihu, T., Prikk, A., Rootamm, R., Konist, A. Comparison of ash from PF and CFB boilers and behaviour of ash in ash fields. In: *Proceedings of the 20th International Conference on Fluidized Bed Combustion*, May 18–21, 2009, Xi'an, China. Springer, Berlin, Heidelberg, 2010.
23. Kuusik, R., Uibu, M., Kirsimäe, K., Mõtlep, R., Meriste, T. Open-air deposition of Estonian oil shale ash: formation, state of art, problems and prospects for the abatement of environmental impact. *Oil Shale*, 2012, **29**(4), 376–403. https://doi.org/10.3176/oil.2012.4.08
24. Paaver, P., Paiste, P., Liira, M., Kirsimäe, K. Mechanical activation of the Ca-rich circulating fluidized bed combustion fly ash: development of an alternative binder system. *Minerals*, 2021, **11**(1), 3. https://doi.org/10.3390/Min11010003
25. Liira, M., Kirsimäe, K., Kuusik, R., Mõtlep, R. Transformation of calcareous oil-shale circulating fluidized-bed combustion boiler ashes under wet conditions. *Fuel*, 2009, **88**(4), 712–718. https://doi.org/10.1016/j.fuel.2008.08.012
26. Kuusik, R., Paat, A., Veskimäe, H., Uibu, M. Transformations in oil shale ash at wet deposition. *Oil Shale*, 2004, **21**(1), 27–42. https://doi.org/10.3176/oil.2004.1.04
27. Paaver, P., Järvik, O., Kirsimäe, K. Design of high volume CFBC fly ash based calcium sulphoaluminate type binder in mixtures with ordinary Portland cement. *Materials*, 2021, **14**(19). https://doi.org/10.3390/ma14195798
28. Ben Haha, M., Winnefeld, F., Pisch, A. Advances in understanding ye'elimite-rich cements. *Cem. Concr. Res.*, 2019, **123**, 105778. https://doi.org/10.1016/j.cemconres.2019.105778
29. Glasser, F. P., Zhang, L. High-performance cement matrices based on calcium sulfoaluminate–belite compositions. *Cem. Concr. Res.*, 2001, **31**(12), 1881–1886. https://doi.org/10.1016/S0008-8846(01)00649-4
30. Hargis, C. W., Telesca, A., Monteiro, P. J. M. Calcium sulfoaluminate (ye'elimite) hydration in the presence of gypsum, calcite, and vaterite. *Cem. Concr. Res.*, 2014, **65**, 15–20. https://doi.org/10.1016/j.cemconres.2014.07.004
31. Juenger, M. C. G., Winnefeld, F., Provis, J. L., Ideker, J. H. Advances in alternative cementitious binders. *Cem. Concr. Res.*, 2011, **41**(12), 1232–1243. https://doi.org/10.1016/j.cemconres.2010.11.012
32. Telesca, A., Marroccoli, M., Pace, M. L., Tomasulo, M., Valenti, G. L., Monteiro, P. J. M. A hydration study of various calcium sulfoaluminate cements. *Cem. Concr. Compos.*, 2014, **53**, 224–232. https://doi.org/10.1016/j.cemconcomp.2014.07.002
33. Myneni, S. C. B., Traina, S. J., Logan, T. J. Ettringite solubility and geochemistry of the $Ca(OH)_2$–$Al_2(SO_4)_3$–H_2O system at 1 atm pressure and 298 K. *Chem.*

Geol., 1998, **148**(1–2), 1–19. https://doi.org/10.1016/S0009-2541(97)00128-9
34. Leben, K., Mõtlep, R., Paaver, P., Konist, A., Pihu, T., Kirsimäe, K. Geochemical study of stable carbon and oxygen isotopes in landfilled Ca-rich oil shale ash. *Est. J. Earth Sci.*, 2020, **69**(3), 134–142. https://doi.org/10.3176/earth.2020.09
35. Leben, K., Mõtlep, R., Konist, A., Pihu, T., Kirsimäe, K. Carbon dioxide sequestration in power plant Ca-rich ash waste deposits. *Oil Shale*, 2021, **38**(1), 65–88. https://doi.org/10.3176/oil.2021.1.04
36. Usta, M. C., Yörük, C. R., Uibu, M., Hain, T., Gregor, A., Trikkel, A. CO_2 curing of Ca-rich fly ashes to produce cement-free building materials. *Minerals*, 2022, **12**(5), 513. https://doi.org/10.3390/min12050513